Article

Kinetics and Mechanical Characterization of Hard Layers Obtained by Boron Diffusion in 80/20 Nickel–Chromium Alloy

Alexis Chino-Ulloa [1], Pablo Alfredo Ruiz-Trabolsi [1], Itzel Pamela Torres-Avila [1], Carlos Orozco-Álvarez [1], Raúl Tadeo-Rosas [2], Julio César Velázquez [3,*] and Enrique Hernández-Sánchez [1,*]

1   Departamento de Bioingeniería, Unidad Profesional Interdisciplinaria de Biotecnología, Instituto Politécnico Nacional, México City 07340, Mexico

2   Facultad de Ingeniería Mecánica y Eléctrica, Universidad Autónoma de Coahuila, Unidad Torreón, Torreón Coahuila 27276, Mexico

3   Departamento de Ingeniería Química Industrial, ESIQIE, Instituto Politécnico Nacional, UPALM Edif. 7, Zacatenco, México City 07738, Mexico

*   Correspondence: jvelazqueza@ipn.mx (J.C.V.); enriquehs266@yahoo.com.mx (E.H.-S.); Tel.: +52-1-551-069-2992 (E.H.-S.)

Abstract: This study examines the formation of hard layers containing Ni-B and Cr-B on the surface of 80/20 nickel–chromium alloy. The work evaluates the mechanical properties of the boride layers using instrumented nanoindentation. In addition, the growth kinetics of the coatings were assessed by applying a kinetic model that relates the layer thickness with the experimental parameters of temperature and treatment time. First, the boride layers were achieved using the powder-pack boriding process in a conventional furnace. The treatment time was set at 2, 4, and 6 h at temperatures of 900, 950, and 975 °C, respectively. The microstructure of the layers was analyzed by X-ray diffraction. The thickness of the layers showed a closed correlation with the experimental parameters of time and temperature, and was established between 38.97 and 156.49 μm for 2 h to 900 °C and for 6 h to 975 °C, respectively. The hardness and Young's modulus values agree with those presented in the literature for boriding nickel alloys, being in the range of 1.3 GPa on average and 240 to 270 GPa, respectively. The resulting layers exhibited a characteristic diffusion zone where the hardness values decrease gradually without the typical high hardness gradient observed on borided steels.

Keywords: boriding; surface layers; powder pack; mechanical properties

1. Introduction

The nickel–chromium system reveals that chromium is quite soluble in nickel. It has a maximum soluble rate of 47% at the eutectic temperature, decreasing to nearly 30% at room temperature [1]. This characteristic enables nickel–chromium alloys to be chemically stable at high temperatures and suitable for working at high temperatures. Nickel–chromium alloys show corrosion resistance that could be due to the passive layer on the system that is mainly composed of chromium oxy/hydroxide-like stainless steel [2]. This metal is usually used as a thermal element in furnace manufacturing due to its superb stability under high temperatures. Similarly, these non-ferrous alloys have a large variety of uses, such as in: aircraft gas turbines, steam turbines, medical applications, and equipment parts in the chemical industry [3]. These alloys have become so important in the industry that some of them have commercial names, such as Inconel® and Hastelloy®. Nevertheless, due to their high nickel content, nickel–chromium (Ni–Cr) alloys show poor wear resistance, which is their main disadvantage and the reason for their limited use [4]. Specifically, 80/20 nickel–chromium alloy is well known for its excellent mechanical properties and corrosion resistance [5,6]. The 80/20 nickel–chromium alloy is frequently used for wrought and cast parts for high-temperature applications, as it has better oxidation and hot corrosion resistance than other alloys [7]. In that sense, several researchers have studied how to

improve the surface properties of these materials [8–11]. The thermochemical process of boriding is one alternative for enhancing the surface mechanical properties of metallic materials. Boron atoms are diffused into a metallic matrix to form intermetallic surface compounds during the boriding process [12,13]. Boriding is mainly applied to steel alloys such as tool steels, low and high carbon steels, stainless steels, etc. This process has been widely used for nonferrous metals with excellent results [14–18]. It is expected that a hard surface layer with high wear and corrosion resistance is achieved as a result of the boriding process. Different features, such as the chemical composition of the substrate, the boron potential supplied during the process, temperature, and treatment time, determine the resulting characteristics of the layers [16]. The kinetics of the growth of the boride layers, even in ferrous and nonferrous materials, has been studied by different researchers to explain the diffusion process. Campos et al. have developed a kinetic model that correlates the experimental parameters, such as temperature, treatment time, and boron concentration, with the boride layers [17] in ferrous materials. Most authors agree that the growth of the boride layers occurs as a consequence of boron diffusion perpendicular to the surface of the sample, and Fick's law controls the concentration of boron in the boride layers. The boriding process in this material was performed to improve the wear properties of 80/20 nickel–chromium alloy. The boride layer thickness was established as a function of the different treatment conditions and the relationship between the mechanical properties and the boron concentration of the layers. As a result, in the boriding process of 80/20 nickel–chromium alloy, the diffusion process occurs in two stages. First, the boron concentration tends to be constant along with the boride layers for a determined time. This assumption can be explained because the boride phases tend to be stoichiometric for the thickness and time determined. Then, as the diffusion process continues, the boron concentration decreases linearly to arrive at a zero near the substrate. Therefore, by knowing the boron concentration in the boride layer, it is possible to see the boron concentration in the diffusion zone. The boron concentration can be evaluated by the straight-line slope between the boron concentration in the boride layers and the end of the diffusion zone, where the substrate is not affected by the boriding process. After analyzing all the results obtained, it is possible to conclude that the process studied could be of assistance to the industry, as it would feasibly increase the lifetime of the equipment and the devices.

2. Experimental Details

2.1. Boriding Treatment

Cylindrical samples of 80/20 nickel–chromium alloy (Aceros Carpenter, México City, México), 5 mm in diameter and 4 mm in length, were sequentially polished with 80–600 SiC paper (EXTEC CORPORATION, Enfield CT, USA). After the metallographic process, the samples were cleaned in an ultrasonic bath for 5 min in a mixture of ethanol and distilled water (50/50). After cleaning, the samples were introduced into a stainless steel crucible containing the boron powder source, Hef-Durferrit (DURFERRIT, GmbH, Mannheim, Germany). The chemical composition of the samples is described in Table 1.

Table 1. Chemical composition of the 80/20 nickel–chromium alloy.

Nominal Composition	
Element	**Content (%)**
Chromium	19.50
Silicon	1.25
Iron	0.50
Manganese	0.40
Nickel	Balance

The boriding process was carried out at three different temperatures (900, 950, and 975 °C) for 2, 4, and 6 h each, under atmospheric air conditions. After boriding, the samples were cooled to room temperature inside the furnace to reduce the risk of thermal crashes and the subsequent fracture of the layers [14,15,18]. Standard metallographic techniques were used to prepare the samples for microscopic examination. The thickness of the boride layers was measured by optical examination with a GX-51 optical microscope (Olympus, Center Valley, PA, USA). At least 50 measurements were performed to establish a mean value of the layer thickness.

2.2. Kinetics of Growth

It is well known that boron diffusion controls the kinetics of the growth of boride layers, so the development of layers occurs as a consequence of boron diffusion in a perpendicular direction to the surface of the samples [18–23]. Additionally, the boron concentration in the boride phases is established by the second Fick's law (Equation (1)):

$$\frac{\partial C}{\partial t} D = \frac{\partial^2}{\partial X^2} \tag{1}$$

The second Fick's law predicts how a specimen's concentration changes as a function of time due to its diffusion in a specific medium. The second Fick's law is a partial differential equation expressing the mass's conservation during the diffusion process.

The deduction of the second Fick's law is always complex. Nevertheless, a particular solution can be expressed as:

$$C_{(x,t)} = A + B erf\left(\frac{x}{2\sqrt{D_t}}\right) \tag{2}$$

Then, extracting the layer thickness from the equation, it can be expressed as:

$$x^2 = \left[2\sqrt{D} erf^{-1}\left(\frac{C_{(x,t)} - C_s}{C_0 - C_s}\right)\right]^2 t \tag{3}$$

It is essential to point out that Equation (3) considers a particular case where the boron concentration profile on the boride layer is of a linear function, as shown in Figure 1.
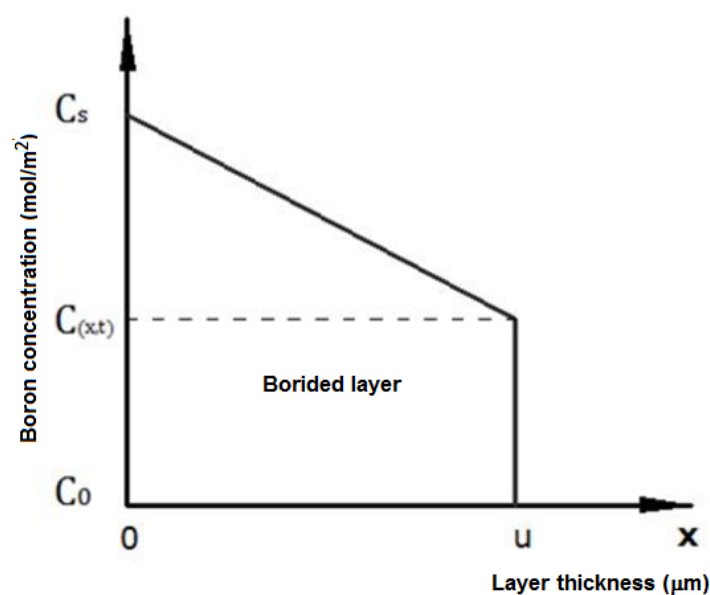

Figure 1. Schematic representation of boron concentration in the boride layers.

where C_s is the boron concentration on the surface of the layer (mol m^{-2}), $C_{(x,t)}$ represents the boron concentration at a distance (x) in time (t) and C_0 (mol m^{-2}) denotes the boron concentration in the substrate. On the other hand, considering that, for distance (x) at any time of treatment (t), the relationship between the boron concentration and the diffusion coefficient tends to be constant (as shown in Figure 1), Equation (3) can be rewritten as:

$$x^2 = Kt \tag{4}$$

Equation (4) indicates that the boride layer's growth obeys a parabolic law [23,24] where (x) is the thickness of the boride layers (m), (K) represents the constant of parabolic growth (m^2/s), and (t) stands for the treatment time (s).

(K) can be estimated from the slope of the graph layer thickness squared (x^2) versus treatment time. The relationship between the constant of parabolic growth (K), temperature (T), and activation energy (Q) can be expressed by an Arrhenius-type equation as follows:

$$K = K_0 \exp(-Q/RT) \tag{5}$$

where (K_0) is called the pre-exponential constant, (Q) denotes the activation energy required to make the reaction occur (J mol^{-1}), and (T) refers to the absolute temperature (Kelvin). In addition, (R) is the constant of ideal gases (8.3144 J mol^{-1} K^{-1}).

The activation energy can be estimated by plotting Equation (5) in a logarithm form as follows:

$$\ln K = \ln K_0 - (Q/R)/\text{T} \tag{6}$$

2.3. Characterization

The thicknesses of the boride layers were measured using the methodology described in Figure 2. At least 100 measurements were realized in 10 different zones of the boride samples.
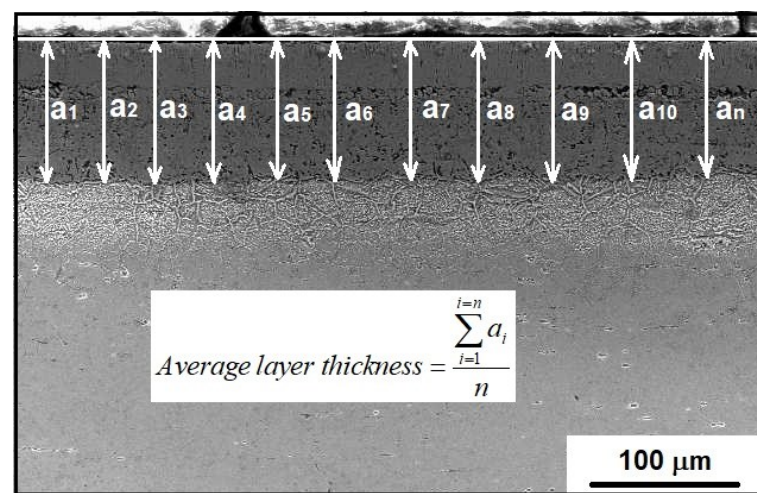

Figure 2. Methodology for layer thickness determination.

The hardness and Young's modulus of the boride layers were evaluated by instrumented indentation with a nanohardness tester (TTX-NHT, CSM Instruments, Needham, MA, USA) using a Berkovich indenter, according to the methodology established by Oliver and Pharr [21]. The hardness profiles were realized at each 25 μm from the surface to the substrate, 10 indentations with a constant indentation load of 250 mN each

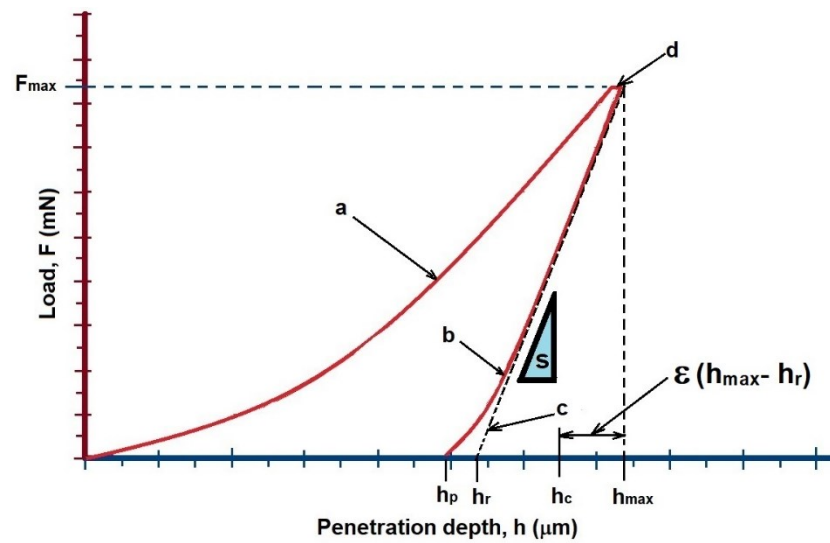The instrumented indentation technique is based on the curve load deformation generated during the test (Figure 3).

Figure 3. Schematic indentation curve obtained using a Berkovich nanoindenter: a is the curve of application of load F; b is the curve of removal of load F; c is the tangent to curve b at F_{max}; d is the dwell period to F_{max}, F is the test load; F_{max} is the maximal test load; h_p is the permanent indentation depth; h_r is the tangent indentation depth; h_c is the contact depth of the indenter with the sample at F_{max}; h_{max} is the maximum indentation depth; S is the contact stiffness; and ε is a geometric constant related to the shape of the indenter, according to the methodology established by Oliver and Pharr [21].

In the nanohardness test, the hardness values were obtained by measuring the depth of the indentation where the indenter is in contact with the material. This is because, at this level of load, the material experiences an elastic recovery, so the permanent indentation print does not indicate the real penetration of the indenter. Figure 4 shows a schematic of the measurement of the contact depth during the indentation test.
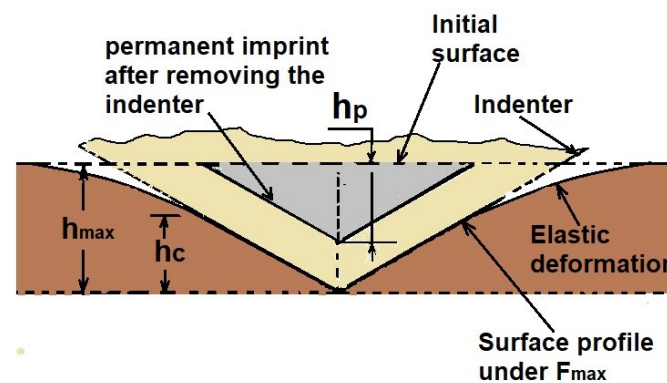
Figure 4. Schematic representation of indenter-sample contact during the indentation test.

The resulting load-displacement response typically shows an elastic-plastic loading followed by elastic unloading (see Figure 3).

The elastic equations of contact are then used in conjunction with the unloading data to determine the Young's modulus and hardness of the specimen material as follows:

$$H = \frac{F_{max}}{A_c} \tag{7}$$

$$E = \frac{1 - v_s^2}{(1/E_r) - \left((1 - v_i^2)/E_i\right)} \tag{8}$$

$$E_r = \frac{\sqrt{\pi S}}{2\beta \sqrt{A_c(h_c)}} \tag{9}$$

where (H) is the hardness of the specimen, F_{max} refers to the maximum applied load, A_c stands for the contact area at peak load ($24.49\ h_c^2$), h_c denotes the experimentally measured contact indentation depth, 24.49 is a constant related to the geometry of the indenter, E is the Young's modulus, v_s represents the Poisson's ratio of the sample (0.3), v_i stands for the Poisson's ratio of the indenter (0.07 for diamond), E_i denotes the Young's modulus of the indenter (1141 GPa), E_r represents a reduced modulus of the indentation contact, and S is the stiffness of the sample [25].

The presence and nature of the boride layers were evidenced by scanning electron microscopy (SEM) (JSM-6360LV, JEOL, JEOL Ltd., Akishima, Japan), using 20 kV of energy, and were corroborated by X-ray diffraction (XRD) using a D8 FOCUS diffractometer (Bruker, Billerica, MA, USA) equipped with Cu-K radiation (1.5418 Å).

3. Results and Discussions

3.1. Microstructure

SEM examination (JSM-6360LV, JEOL, JEOL Ltd., Akishima, Japan) of a cross-section of the borided samples revealed the presence of three zones of interest (Figure 5). The outermost is assumed to be a layer containing Ni-B and Cr-B compounds with flat morphology, similar to borided stainless steel [15,21]. The second is a large diffusion zone and the substrate, which is not affected by the diffusion process.
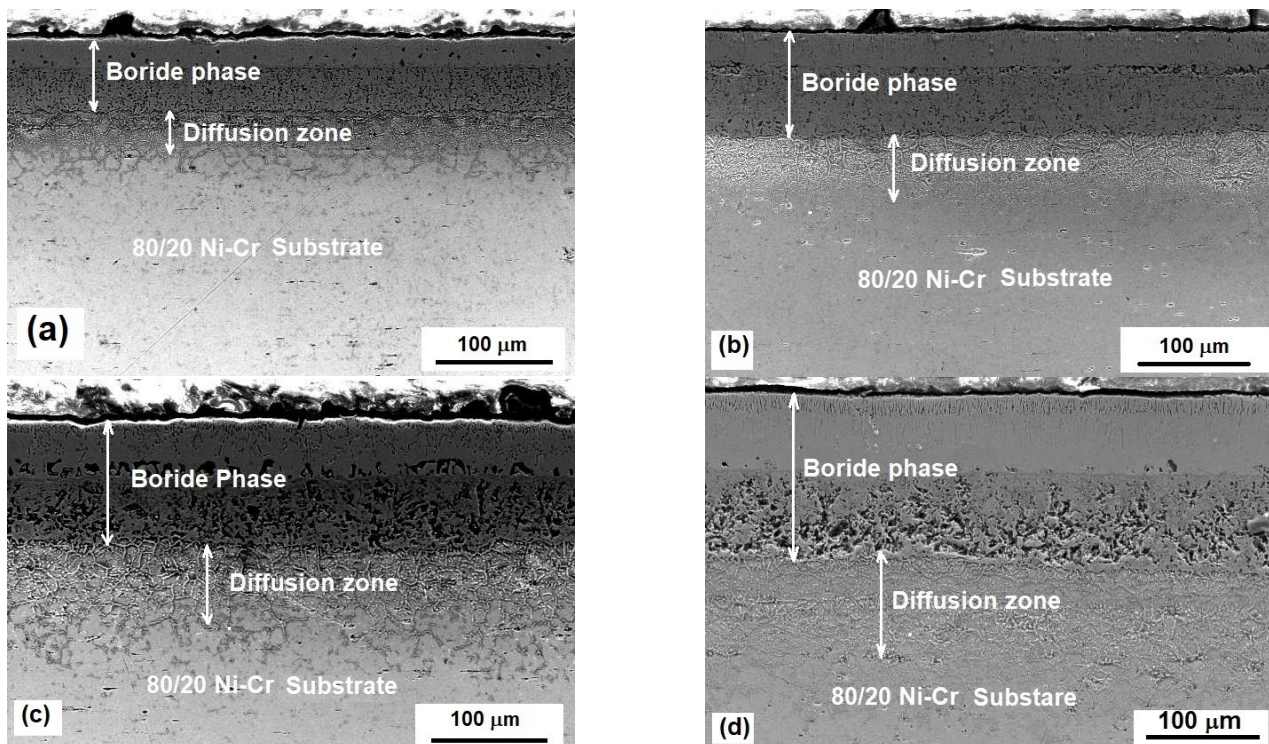

Figure 5. *Cont.*
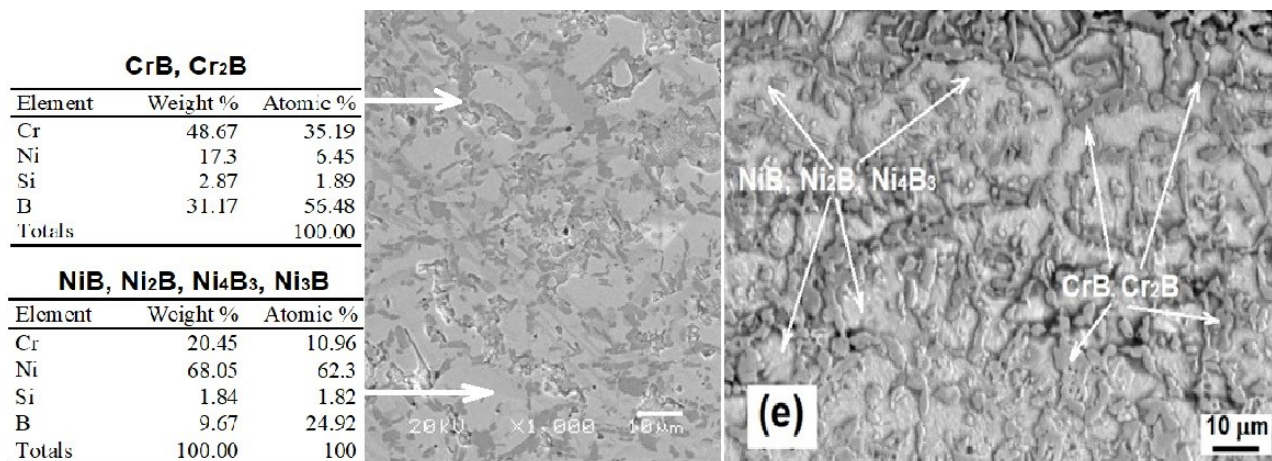
CrB, Cr₂B		
Element	Weight %	Atomic %
Cr	48.67	35.19
Ni	17.3	6.45
Si	2.87	1.89
B	31.17	55.48
Totals		100.00

NiB, Ni₂B, Ni₄B₃, Ni₃B		
Element	Weight %	Atomic %
Cr	20.45	10.96
Ni	68.05	62.3
Si	1.84	1.82
B	9.67	24.92
Totals	100.00	100

Figure 5. SEM microphotography of a cross-section of the 80/20 nickel–chromium alloy, borided at 900 °C for 2 and 6 h (**a**,**c**), 975 °C for 2 h (**b**), and 975 °C for 6 h (**d**,**e**).

As shown in Figure 5, the thickness of the layers depends not only on the temperature, but also on the treatment time (see Table 2). The layers with the lowest thickness are those exposed to the lowest temperature for the shortest time (900 °C and 2 h). Therefore, once the temperature necessary for boron mobility is reached, the layer starts to grow and continues growing during the process [24]. This behavior confirms the assumption that boriding is a thermally activated process.

Table 2. Layer thickness as a function of the treatment parameters (µm).

	Temperature (°C)		
Time (h)	900	950	975
2	39 ± 2.8	63 ± 5.2	100 ± 08.8
4	68 ± 4.5	989 ± 8.7	131 ± 12.4
6	86 ± 9.2	123 ± 10.1	156 ± 14.3

The flat morphology of the boride layers (similar to those obtained in stainless steel) can be explained because of the high Cr content in the alloy. It has been shown that the high contents of Cr and Ni in the alloys exposed to boriding tend to act as a diffusion barrier, limiting the growth of the layers and consuming high amounts of energy during the process [15].

On the other hand, the thickness of the layers obtained on the alloys containing Ni-Cr will be lower than those obtained in low-alloyed steel under the same treatment conditions. Similar results were reported by Campos et al. [26], even when they used a different technique for the boriding process to accelerate the growth of the layers.

A dendritic phase can be observed in the microstructure (Figure 5e), which is assumed to be chromium borides (CrB and Cr₂B), while the brighter phase corresponds to NiB, Ni₂B, and Ni₄B₃ [23]. Interesting results were obtained from the elementary analysis applied to the dendritic and to the brighter phases (Figure 5e). The boron content in the dendritic phase was near to 50% (atomic content), which means that the main structure in this phase is CrB with a 50/50% atomic composition. The low content of Ni indicates that Ni was displaced with the Cr-B structures. Additionally, when the brighter phases were analyzed, the boron content matched better with the Ni₃B structure, and the Cr content was reduced due to the Ni-B compound formation.

The XRD analysis corroborated the composition of the boride layers, as shown in Figure 6.
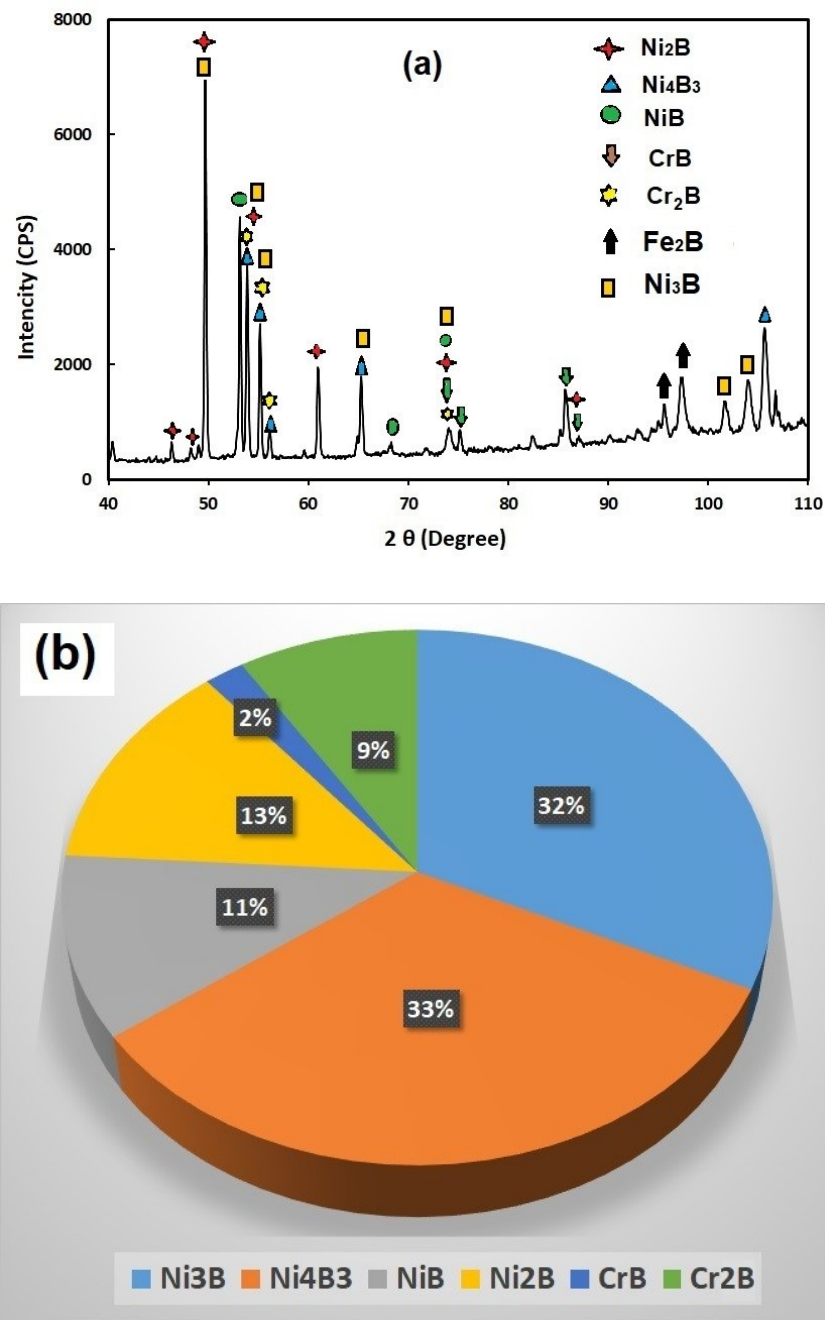
Figure 6. XRD pattern applied on the surface of the 80/20 nickel–chromium alloy borided at 975 °C for 6 h (**a**); and the distribution of the boride phases in the layers according to the XRD analysis (**b**).

The XRD analysis (Figure 6a) revealed the presence of Ni-B and Cr-B characteristic peaks. Indications of NiB, Ni_4B_3, Ni_2B, Ni_3B, CrB, and Cr_2B were evidenced. Interestingly, even though the alloy contains only 0.5% by weight of iron (Table 1), some indications of iron boride type Fe_2B can be observed in the XRD analysis. The presence of iron borides in the boride layer indicates the affinity of iron to boron. According to the XRD analysis (Figure 6b), the layer is mainly compounded by Ni_4B_3 and Ni_3B. The results indicate how the boron concentration decreases through the boride layer until it reaches the diffusion zone and finally approaches zero. This behavior confirms the assumption that the concentration profile on the boride layer is of a linear function (Figure 1). The formation of this type of boron compound enhances the surface properties of the treated material, such as the hardness, Young's modulus, corrosion resistance, and wear resistance [8,10,23]. A probable

explanation for the improvement in the mechanical properties could be the combination of Ni-B and Cr-B, which have a hardness of approximately 1300 to 2400 HV [23].

3.2. Kinetics of Growth

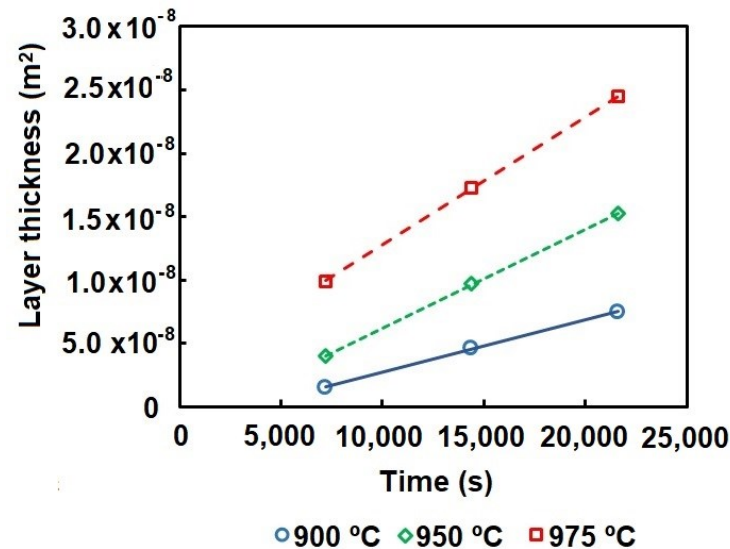The mean values of the layer thickness are depicted in Table 2 and shown in Figure 7.

Figure 7. Behavior of the layer thickness as a function of the treatment time for each temperature.

The results show how the thickness of the layer evolves as a function of the temperature and treatment time. The most relevant parameter is the temperature because the layer thickness increases as the temperature increases; for example, from 38.97 ± 2.8 µm for 2 h and 900 °C to 99.68 ± 08.8 µm for 2 h and 975 °C. This behavior confirms the affinity of nickel to boron since it is possible to obtain boride layers even faster than in low carbon steels [24]. On the other hand, it is clear that the layer thickness evolves as a function of the treatment time. However, at low treatment time and temperature, the layer's thickness is low due to the layer's growth requiring a certain time to start. This time necessary for initiating the layer's growth is known as incubation time, and its effect is more evident at low temperatures (see Table 2).

The values of the parabolic growth constant (K) were estimated using the slope of the curves (Figure 7); their values are summarized in Table 3.

Table 3. Parabolic growth constant values for different treatment conditions.

Temperature	K	R
(°C)	(m^2/s)	-
900	4.14×10^{-13}	0.9910
950	7.80×10^{-13}	0.9998
975	1.01×10^{-12}	0.9918

According to the values shown in Table 3, it is feasible to consider that the values of K are correct due to the excellent correlation of the points to a straight line. The results indicate that the boriding process of the 80/20 nickel–chromium alloy is a controlled process, where the growth of the layers is directly dependent on the treatment parameters, such as temperature and time.

The values of the parabolic growth constant were concordant with those reported by Campos et al. [26], even when they used an electrochemical method to accelerate the process.

Once the parabolic growth constant for the borided 80/20 nickel–chromium alloy was estimated, it was possible to assess the activation energy (Q) necessary for boron mobility during the boriding process. Therefore, the activation energy was calculated by plotting the Arrhenius equation in logarithmic form (Figure 8), and estimated to be 145.9 kJmol^{-1}.
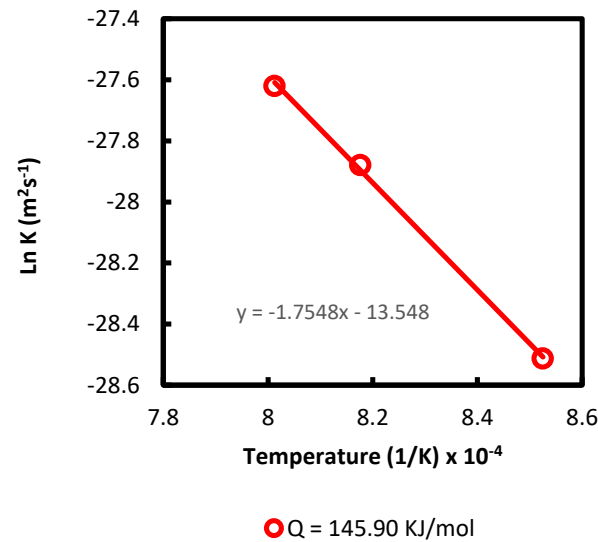

y = -1.7548x - 13.548

Q = 145.90 KJ/mol

Figure 8. Behavior of the parabolic growth constant as a function of the treatment temperature.

This result was compared with those reported in the literature (Table 4) for nickel alloys, such as Ni$_3$Al, and borided steels [23,27–29].

Table 4. Different activation energy values are achieved for different materials exposed to the boriding process.

Material	Activation energy (KJ/mol)	Reference
Ni$_3$Al	188.8	[23]
AISI W1	171.2	[28]
AISI 4140	215.0	[29]
80/20 Ni–Cr	145.3	[present]

The 80/20 nickel–chromium alloy (present work) requires the lowest activation energy to diffuse boron and to form compounds such as Ni-B and Cr-B. This means that it is possible to enhance the surface properties of 80/20 nickel–chromium alloy at a relatively low cost.

The pre-exponential constant (K_0) was estimated through the intersection of the ordinated axis, and was evaluated as 1.31×10^{-6} m^{2}s^{-1}.

The values of (K_0) and (Q) determined from the experimental results can be used to propose a particular solution to the diffusion process applied to 80/20 nickel–chromium alloy, so Equation (10) can be rewritten as:

$$K = 1.3 \times 10^{-6} \exp\left(\frac{-17548}{T}\right) \tag{10}$$

where K is the growth rate, and T represents the treatment's absolute temperature (Kelvin). By analyzing Equations (4) and (10), it is possible to develop a practical formula for estimating the layer thickness under pre-determined treatment conditions. Equation (4) can be rewritten as:

$$x = \sqrt{1.31 \times 10^{-6} \exp\left(\frac{-17548}{T}\right) t} \tag{11}$$

According to the results presented in Table 5, the data calculated show specific errors, especially at a short treatment time. However, the errors decrease as the temperature and treatment time increase. This behavior can be explained because the boriding process depends on the treatment parameters. Therefore, as the time and temperature increase, the process becomes more stable, and the model becomes more efficient. One way to diminish the error could be to add one more time and temperature condition, and eliminate the first condition (2 h and 900 °C). Finally, once stabilized, the model (Equation (11)) calculates the first condition data and compares it with the experimental data.

Table 5. Comparison of the experimental values and those estimated by Equation (10).

	900 °C			950 °C			975 °C		
	Layer Thickness (µm)			Layer Thickness (µm)			Layer Thickness (µm)		
Time (s)	Measured	Calculated	Error (%)	Measured	Calculated	Error (%)	Measured	Calculated	Error (%)
7200	38.97	54.80	40.62	63.21	74.41	17.71	99.68	85.90	13.81
14,400	68.08	77.50	13.84	98.79	105.22	6.51	131.47	121.49	7.59
21,600	86.48	94.92	9.76	123.39	128.87	4.44	156.49	148.79	4.92

3.3. Mechanical Characterization

The hardness and Young's modulus were estimated by instrumented indentation.

The indentations were performed perpendicularly to the diffusion surface. Only the indentations with suitable geometry were considered for measurement.

Once the boride layers were observed (Figure 5), it was decided to make the indentations starting at 25 µm from the surface and every 25 µm until reaching the substrate. The above because from 25 µm, there is a consolidated phase of borides, in all treatment conditions.

The hardness behavior of the boride layers is shown in Figure 9. As can be observed, the hardness values of the layers tended to increase as the temperature and treatment time increased. This behavior can be attributed to the enrichment of the layers with boron as the process evolves. The results show that the layers are more compact and the compounds formed tend to be saturated until the equilibrium is reached. The hardness profiles presented in Figure 9 show a gradually reduction in hardness, and this behavior indicates that the hardness of the boride layers is highly dependent on the boron concentration. Thus, according to the model presented in Figure 1, the boron concentration in the boride layer is higher on the surface and decreases gradually to the substrate. The results match well with the layer's thicknesses presented in Table 2, where the slope of the hardness gradient is more pronounced for the samples exposed to 900 °C than for those exposed to 975 °C, indicating a gradient of concentration that decreases from the surface to the substrate.

The highest hardness value was 1360 ± 70 HV near to the surface of the sample exposed to 975 °C for 6 h. Compared with the hardness of the 80/20 nickel–chromium alloy (270 ± 12 HV) achieved directly from the measured values, the increase in the hardness values at the surface of the 80/20 nickel–chromium alloy indicates an excellent improvement in its mechanical surface.

The behavior of the Young's modulus as a function of the different treatment conditions is shown in Figure 10.
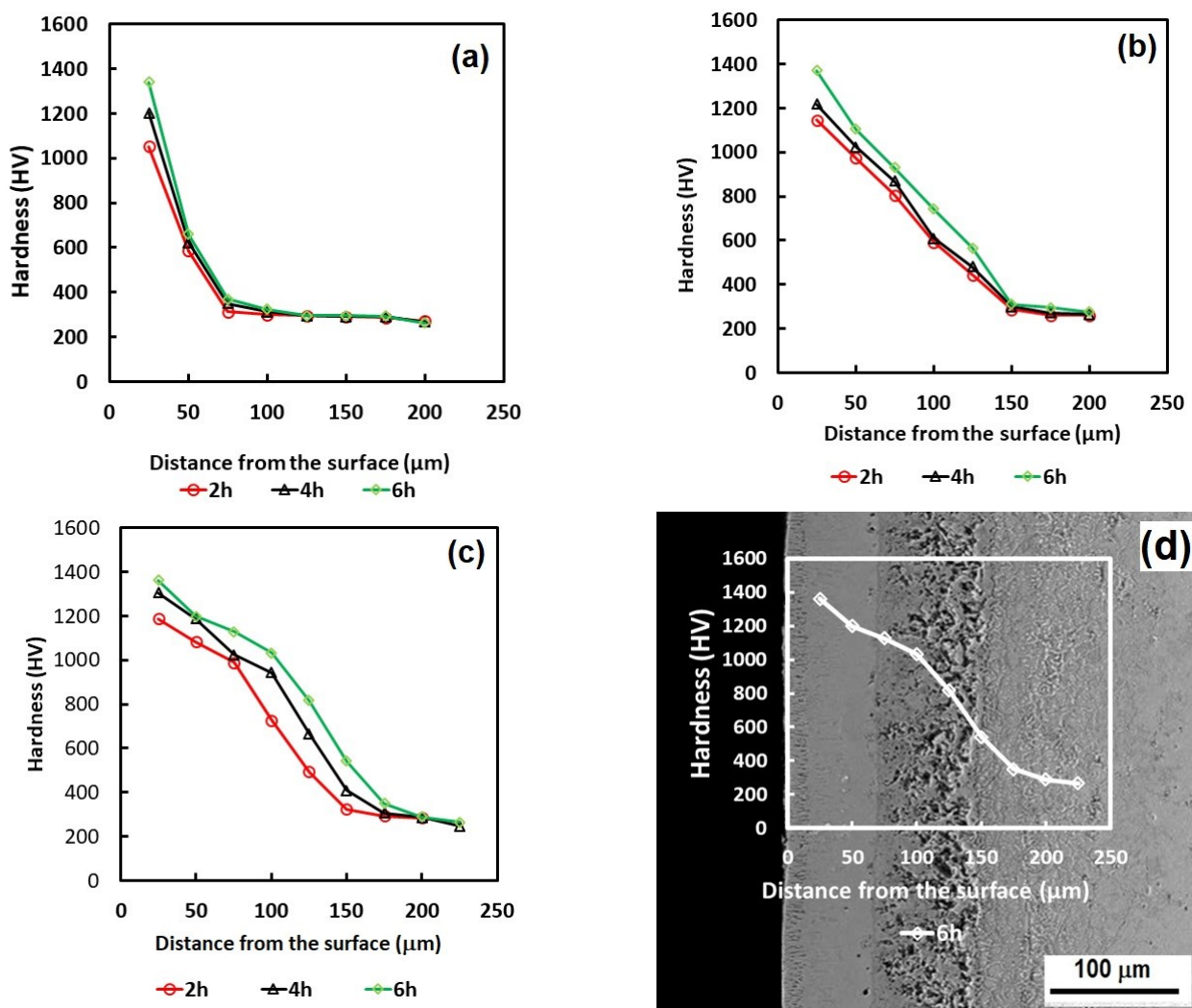
Figure 9. Hardness behavior for 900 °C, 950 °C and 975 °C (**a**–**c**) respectively. (**d**) represents the zones where the hardness profiles were measured (Sample exposed to 975 °C for 6 h).
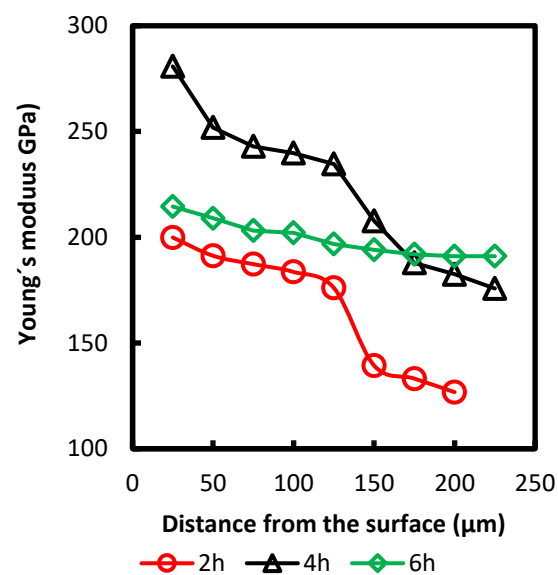

Figure 10. The behavior of the Young's modulus for the samples exposed to 975 °C for 2, 4, and 6 h.

The Young's modulus increased from 168 ± 27 GPa in the substrate (measured directly from the material) to 270 ± 20 GPa near the boride phase's surface.

The results where compared with those reported in literature. For example, Kulka et al. reported 343 GPa for Inconel 600 alloy borided by laser boriding [23]. In all probability, the difference can obey the Fe content between the Inconel 600 alloy and the 80/20 nickel–chromium alloy, since the iron borides reported by them increase the hardness and the Young's modulus of the surface phase.

Makuch reported a Young's modulus of 232 GPa for nickel borides exposed to gas boriding. Makuch [10] exposed Nisil alloy to gas boriding to 910 °C for 2 h, and the results are concordant with those of the present study.

The increase in Young's modulus presumably represents a decrease in the ductility of the material, as the behavior of the boride layer is similar to that exhibited by a ceramic material (high hardness and high brittleness), especially considering that its main applications are in the field of heater elements. However, according to the results, the increase in hardness and Young's modulus occurs gradually, so the material will not suffer damage during the manufacturing process.

4. Conclusions

The following conclusions can be derived from the present study:

1. The boride layers' growth in 80/20 Ni–Cr alloy obeys parabolic law, so the boriding process can be considered a controlled process.
2. The layer thickness depends on the treatment conditions, time, and temperature. However, the temperature of the process seems to be the most relevant parameter, since a low increase in temperature generated high changes in the growth rate of the boride layers.
3. The hardness of the boride layers is also dependent on the treatment conditions and was established in the range from 1052 to 1350 HV, compared with the hardness of the substrate which is approximately 270 HV. Moreover, the hardness of the boride phase decreases gradually as a function of the distance from the surface, indicating a decrease in the boron concentration.
4. The activation energy for the mobility of boron into 80/20 Ni–Cr alloy was established as 145.9 kJ/mol, which is similar to that reported for the low-alloying steels. The result indicates that 80/20 Ni–Cr alloy has an excellent affinity to boron diffusion.

Author Contributions: Conceptualization, E.H.-S. and J.C.V.; methodology, P.A.R.-T.; validation, E.H.-S.; formal analysis, A.C.-U.; investigation, R.T.-R.; resources, E.H.-S.; data curation, I.P.T.-A. and C.O.-Á.; writing—original draft preparation, A.C.-U. and P.A.R.-T.; writing—review and editing, E.H.-S. and J.C.V.; visualization, E.H.-S.; supervision, I.P.T.-A.; project administration, E.H.-S. and J.C.V.; funding acquisition, E.H.-S. All authors have read and agreed to the published version of the manuscript.

Institutional Review Board Statement: Not applicable.

Informed Consent Statement: Not applicable.

Data Availability Statement: Not applicable.

Conflicts of Interest: The authors declare no conflict of interest.

References

1. Gossé, S. Thermodynamic Assessment of Solubility and Activity of Iron, Chromium, and Nickel in Lead Bismuth Eutectic. *J. Nucl. Mater.* **2014**, *449*, 122–131. [CrossRef]
2. Metikoš-Huković, M.; Omanović, S.; Babić, R.; Milošev, I. An Electrochemical Study of the Passive Film Formed on Ni-Cr (80/20) Coating. *Ber. Bunsenges. Phys. Chem.* **1994**, *98*, 1243–1249. [CrossRef]
3. Nickel and Nickel Alloys. Available online: http://www.totalmateria.com/Article9.htm (accessed on 18 July 2022).

4.   Aytekin, H.; Akçin, Y. Characterization of Borided Incoloy 825 Alloy. *Mater. Des.* **2013**, *50*, 515–521. [CrossRef]
5.   Stott, F.H.; Lin, D.S.; Wood, G.C.; Stevenson, C.W. The Tribological Behaviour of Nickel and Nickel-Chromium Alloys at Temperatures from 20° to 800 °C. *Wear* **1976**, *36*, 147–174. [CrossRef]
6.   Bond, A.P.; Uhlig, H.H. Corrosion Behavior and Passivity of Nickel-Chromium and Cobalt-Chromium Alloys. *J. Electrochem. Soc.* **1960**, *107*, 488. [CrossRef]
7.   Viswanathan, R. High Temperature Corrosion of Some Gas Turbine Alloys. *Corrosion* **1968**, *24*, 359–368. [CrossRef]
8.   Makuch, N.; Kulka, M.; Dziarski, P.; Taktak, S. The Influence of Chemical Composition of Ni-Based Alloys on Microstructure and Mechanical Properties of Plasma Paste Borided Layers. *Surf. Coat. Technol.* **2019**, *367*, 187–202. [CrossRef]
9.   Ge, H.; Yang, Y.; Zheng, S.; Liu, K.; Ma, X. Creep Induced Precipitation of the $(Cr,Mo)5B3$-Type Boride in γ/Γ' Eutectic of a Ni-Based Superalloy. *Mater. Character.* **2020**, *169*, 110569. [CrossRef]
10.   Makuch, N. Influence of Nickel Silicides Presence on Hardness, Elastic Modulus and Fracture Toughness of Gas-Borided Layer Produced on Nisil-Alloy. *Trans. Nonferrous Met. Soc. China* **2021**, *31*, 764–778. [CrossRef]
11.   Galerie, A. High Temperature Corrosion of Chromia-Forming Iron, Nickel and Cobalt-Base Alloys. In *Shreir's Corrosion*; Elsevier: Amsterdam, The Netherlands, 2010; pp. 583–605. [CrossRef]
12.   Hernández-Sanchez, E.; Rodriguez-Castro, G.; Meneses-Amador, A.; Bravo-Bárcenas, D.; Arzate-Vazquez, I.; Martínez-Gutiérrez, H.; Romero-Romo, M.; Campos-Silva, I. Effect of the Anisotropic Growth on the Fracture Toughness Measurements Obtained in the Fe_2B Layer. *Surf. Coat. Technol.* **2013**, *237*, 292–298. [CrossRef]
13.   Velázquez-Altamirano, J.C.; Torres-Avila, I.P.; Teran-Méndez, G.; Capula-Colindres, S.I.; Cabrera-Sierra, R.; Carrera-Espinoza, R.; Hernández-Sánchez, E. A Stochastic Model and Investigation into the Probability Distribution of the Thickness of Boride Layers Formed on Low-Carbon Steel. *Coatings* **2019**, *9*, 756. [CrossRef]
14.   Hernández-Sánchez, E.; Domínguez-Galicia, Y.M.; Orozco-Álvarez, C.; Carrera-Espinoza, R.; Herrera-Hernández, H.; Velázquez, J.C. A Study on the Effect of the Boron Potential on the Mechanical Properties of the Borided Layers Obtained by Boron Diffusion at the Surface of AISI 316L Steel. *Adv. Mater. Sci. Eng.* **2014**, *2014*, 249174. [CrossRef]
15.   von Matuschka, M.G. *Boronizing*, 1st ed.; Carl Hanser: Munich, Germany, 1980.
16.   Campos, I.; Bautista, O.; Ramírez, G.; Islas, M.; de La Parra, J.; Zúñiga, L. Effect of Boron Paste Thickness on the Growth Kinetics of Fe_2B Boride Layers during the Boriding Process. *Appl. Surf. Sci.* **2005**, *243*, 429–436. [CrossRef]
17.   Campos-Silva, I.; Ortiz-Domínguez, M.; Bravo-Bárcenas, O.; Doñu-Ruiz, M.A.; Bravo-Bárcenas, D.; Tapia-Quintero, C.; Jiménez-Reyes, M.Y. Formation and Kinetics of FeB/Fe_2B Layers and Diffusion Zone at the Surface of AISI 316 Borided Steels. *Surf. Coat. Technol.* **2010**, *205*, 403–412. [CrossRef]
18.   Ozbek, I.; Bindal, C. Kinetics of Borided AISI M2 High Speed Steel. *Vacuum* **2011**, *86*, 391–397. [CrossRef]
19.   Popela, T.; Vojtěch, D. Characterization of Pack-Borided Last-Generation TiAl Intermetallics. *Surf. Coat. Technol.* **2012**, *209*, 90–96. [CrossRef]
20.   Gurappa, I. Development of Appropriate Thickness Ceramic Coatings on 316 L Stainless Steel for Biomedical Applications. *Surf. Coat. Technol.* **2002**, *161*, 70–78. [CrossRef]
21.   Oliver, W.C.; Pharr, G.M. An Improved Technique for Determining Hardness and Elastic Modulus Using Load and Displacement Sensing Indentation Experiments. *J. Mater. Res.* **1992**, *7*, 1564–1583. [CrossRef]
22.   Özbek, I.; Konduk, B.A.; Bindal, C.; Ucisik, A.H. Characterization of Borided AISI 316L Stainless Steel Implant. *Vacuum* **2002**, *65*, 521–525. [CrossRef]
23.   Kulka, M.; Makuch, N.; Dziarski, P.; Piasecki, A. A Study of Nanoindentation for Mechanical Characterization of Chromium and Nickel Borides' Mixtures Formed by Laser Boriding. *Ceram. Internat.* **2014**, *40*, 6083–6094. [CrossRef]
24.   Hernández-Sánchez, E.; Velázquez, J.C. Kinetics of Growth of Iron Boride Layers on a Low-Carbon Steel Surface. In *Laboratory Unit Operations and Experimental Methods in Chemical Engineering*; InTech: London, UK, 2018. [CrossRef]
25.   ASTM International ASTM E384. *Standard Test Method for Microindentation Hardness of Materials*; ASTM: West Conshohocken, PA, USA, 2013.
26.   Campos-Silva, I.; Hernández-Ramirez, E.J.; Contreras-Hernández, A.; Rosales-Lopez, J.L.; Valdez-Zayas, E.; Mejía-Caballero, I.; Martínez-Trinidad, J. Pulsed-DC Powder-Pack Boriding: Growth Kinetics of Boride Layers on an AISI 316 L Stainless Steel and Inconel 718 Superalloy. *Surf. Coat. Technol.* **2021**, *421*, 127404. [CrossRef]
27.   D'Souza, B.; Leong, A.; Yang, Q.; Zhang, J. Corrosion Behavior of Boronized Nickel-Based Alloys in the Molten Chloride Salt. *Corros. Sci.* **2021**, *182*, 109285. [CrossRef]
28.   Genel, K.; Ozbek, I.; Bindal, C. Kinetics of Boriding of AISI W1 Steel. *Mat. Sci. Eng. A* **2003**, *347*, 311–314. [CrossRef]
29.   Sen, S.; Sen, U.; Bindal, C. The Growth Kinetics of Borides Formed on Boronized AISI 4140 Steel. *Vacuum* **2005**, *77*, 195–202. [CrossRef]